Automation 2011 The 11th International Conference on Automation Technology, Douliou, Yunlin, Taiwan, 2011
Paper No. R069

Humanoid_Development of a Human-size Biomimetic Biped Robot

Jing-Yi Chen, Shao-Fan Wang, Chun-Sheng Chen, Jau-Ching Lu, Wei-Shun Yu, and Pei-Chun Lin*

***Abstract*—We report on the development and system integration of a human-size biped robot. On the hardware side, several topics are addressed, including active joint assignment, mechanism design, mechanical arrangement, mechatronic system layout, system integration, etc. On the software side, two topics are included: (1) walking/turning gait development based on the inverted pendulum model, and (2) dynamical simulation within ADMAS/Matlab environment to preview the performance of the designed gaits. After that, the empirical robot experiments are carried out.**

I. Introduction

Humanoid robotics is one of the robotic fields which draw audience's great attention in recent years [1-5]. Research of the humanoid robot have various aspects; for example, human-robot interaction, actroid, etc. In this paper we would like to focus on the "motion" side; more specifically, design bipedal legs which is capable of performing biped locomotion. The most challenge task in developing a humanoid robot is to generate a stable gait, so lots of research on gait analysis or other related topics [6-9]. The method of producing a human-like gait for biped robots has been proposed [10]. Some control methods for biped robot with stable walking gaits have been reported as well [11-13].

Before applying new designed gaits or control methods to a biped robot for performance evaluation, simulations are usually carried out first to ensure the stability of the designed gait. Thus, preventing a possible damage of the expensive and complicate physical robot, which is composed of lots of sensors, actuators, mechanisms, etc. Buschmann et. al. demonstrates that dynamics simulation is a valuable tool for biped robot hardware and controller design [14], and Hirukawa et. al. shows the correspondence between dynamic simulations and the experiments of biped walking of humanoid robots [15]. Here, instead of developing customized dynamic environment by ourselves, we utilize commercial software ADAMS and Matlab to simulate the designed gait. After that, the designed gaits are applied to our physical robot for experimental evaluation.

Section II briefly reports the leg design, including joint arrangement, mechanical design, and mechatronics subsections. Section III and IV describe the walking and turning trajectory generation, respectively. Section V introduces the simulation work, and Section VI reports the experiment evaluation of walking and turning behaviors. Section VII concludes the work.

This work is supported by National Science Council (NSC), Taiwan, under contract 97-2221-E-002-208-MY3.

Authors are with Department of Mechanical Engineering, National Taiwan University (NTU), No.1 Roosevelt Rd. Sec.4, Taipei, Taiwan. (Corresponding email: peichunlin@ntu.edu.tw)..

II. Leg Design

A. Degree of freedom of the leg

Considering robot design, there always exists trade-offs among active/passive degree of freedoms (DOFs), mobility, flexibility system complexity, and controllability.

Great mobility is the common goal; however, how to select right components is indeed not an easy task. By comparing with various existing humanoid robots around the world, in the current prototype we utilize 12 active DOFs in the whole leg mechanism. As shown in the Figure 1, 3 DOFs, 1 DOF, and 2 DOFs are used at hip joint, knee joint, and ankle joint, respectively.

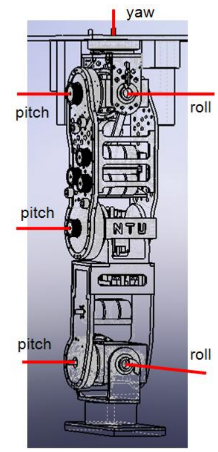

Fig. 1. DOFs of one leg

B. Mechanical Design

Motor Maxon RE-series brushed DC motors are selected based on their high performance and easy interface with general amplifier circuits. The detailed selection of particular models is based on the preliminary static analysis as well as result from Adams simulation.

Harmonic drive Instead of gearbox, harmonic drive is used in our system for major speed reduction due to its excellent performance of limited backlash as well as compact size with high reduction ratio.

Belt and pulley Because of geometrical constraints, it is impossible to connect selected motors to the corresponding harmonic drives directly in the multi-DOF hip and ankle joints. Thus, in these two joints several DOFs are also designed with timing belt-pulley transmission system between the motors and the harmonic drives. In addition, this also preserves the

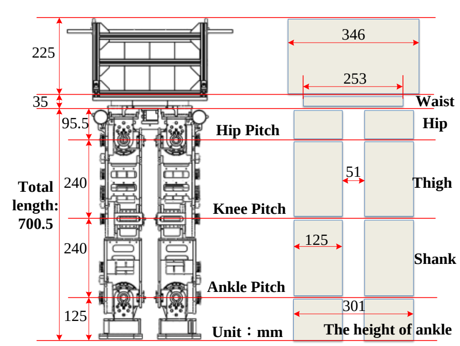

Fig. 2. Dimensions of the biped robot.

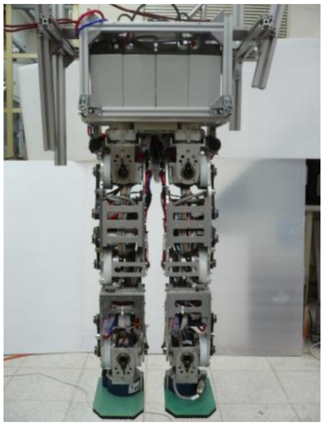

Fig. 3. Picture of the biped robot.

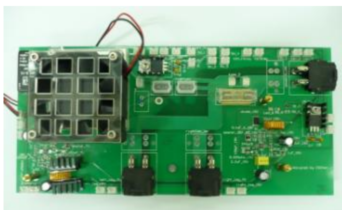

Fig. 4. Power Board.

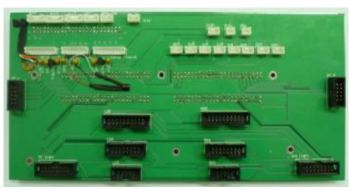

Fig. 5. Break Board.

freedom to adjust the overall speed reduction ratio easily in the future. Idlers are used in the belt-pulley system to maintain the required belt tension as well as to increase the contact areas between the belts and the pulleys which further reduce the load on each tooth.

We have designed and fabricated a biped robot in our laboratory since the project started, and the mechanism model of the biped robot is constructed in SolidWorks shown in Fig. 2, and Fig. 3 is the snapshot of the robot. The robot has 12 degree of freedoms (DOFs), 6 on each leg. The model includes the aluminum structure, motors, Harmonic Drives, pulleys, force sensors and batteries.

C. Mechatronic Design

The Mechatronic of the robot have many parts, such as power board, breakout board, motor drive board units. Then connects to computation center. National Instruments (NI) single-board real-time embedded system (sbRIO) with FPGA is chosen to be the main computation power.

Power Board The power board transforms 48 V to the voltage which the electronic parts need. Figure 4 shows the picture of the power board.

Breakout Board The breakout board collect the signals from the sub-breakout boards and most of the sensors include of six-axis force sensors、inertia measurement unit (IMU) and inclinometer, Fig. 5 is the picture of the breakout board.

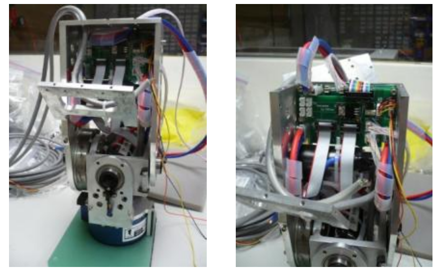

Fig. 6. Disposition chart of custom breakout boards.

Fig. 7. Motor Drive Unit.

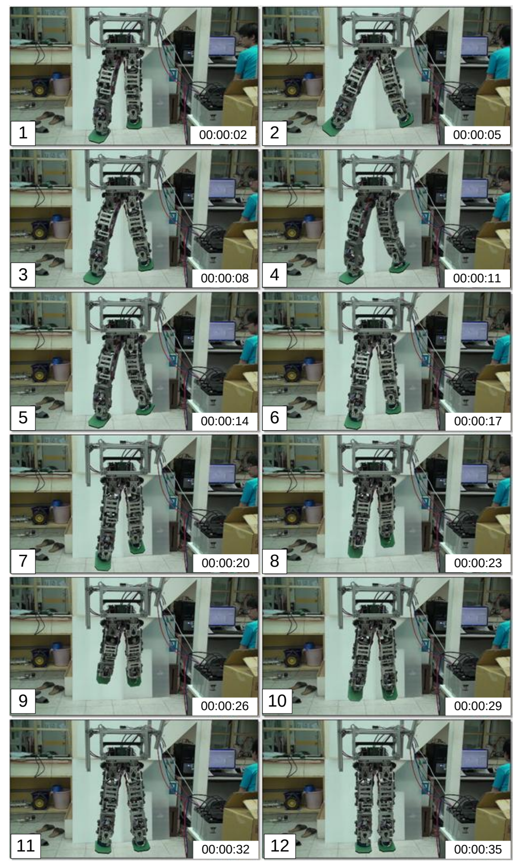

Fig. 8. The snapshots of automatic homing.

Six-axis force sensor Six-axis force sensor is installed between foot and ankle joint which will be the main sensing element to compute the zero-moment point (ZMP) of the contacted foot.

Inertia Measurement Unit (IMU) A traditional 6-axis IMU comprised of three 1-axis gyros (for angular velocity) and one 3-axis accelerometer is also installed, and this sensor provides the essential body-state information of center of mass (COM).

Motor driver board APEX SA60 motor amplifiers are adopted because of their compatibility with selected motors.

The motor drive unit contains a motor drive board and a sub-breakout board. To simplify the electronic layout and wiring, custom breakout boards are designed to be placed next to the motor amplifiers near all driving axes as shown in Figure 6.Due to the rest space of the mechanism and the number of motors, we design six different motor drive units. Fig. 7 is one of the motor drive units.

So far, we have finished the integration between mechanisms and electronic circuits. Before we applied the trajectories to the robot, homing for the robot is a preliminary work because we must make sure that the gesture of robot is straight and can stand on the ground. Figure 8 illustrates the motion of homing. The steps of homing include roll, yaw, pitch orientation, and the motors rotate until the photo interrupters detect the edge of the workspace of the joints, and then the motors rotate reversely back to the homing position. After homing for the robot, we finally finish mechatronic integration and hardware work, and then we can apply the desired trajectories to carry out gait experiments.

III. WALKING TRAJECTORY PLANNING

While biped robot walks stably, not only reaction force between sole and ground and inertia force but also all the moment created by those force must balance, so the ZMP (Zero-Moment Point) of the robot on the sole must lie in the support plane on the ground [8]. In order to simplify dynamic model, there are some assumptions needed to be considered. Furthermore, it is necessary to consider two general phases when robot walks, one is SS (Single Support) phase, and the other is DS (double support) phase. Because the underlying physical principals are different, the trajectory of COM is derived from different dynamic models.

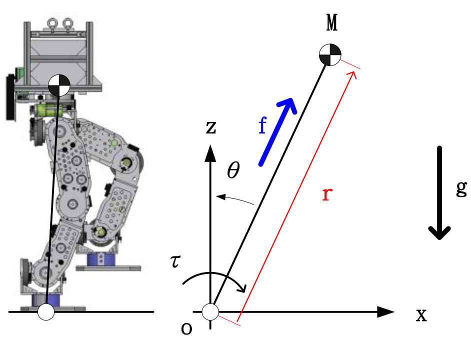

Fig. 9. Inverted pendulum model in sagittal x-z plane.

This section describes how to generate COM trajectories while the robot operates in the SS and DS phases. In the single support phase, the inverted pendulum model is used to generate the trajectory of COM. Figure. 9 explains the simplified model in the sagittal x-z plane, which assumes point mass, weightless leg , and no-slip on the ground.. M is the mass of robot, g represents gravity, r is the vector from the contact point to the center of mass, and τ is zero if the inverted pendulum is a joint contact with ground. In order to reduce the calculation when producing the trajectory, there is a constraint, the height is constant, added to the inverted model, and this

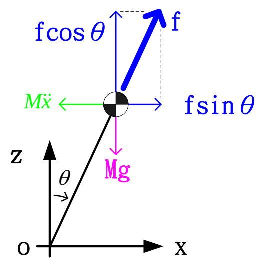

Fig. 10. Free body diagram of the inverted pendulum model constrained with constant height.

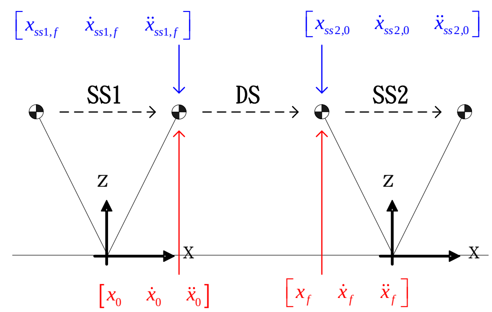

Fig. 11. Generation of the trajectory in the DS phase by polynomial function with given boundary conditions.

model is called a linear inverted pendulum. Figure 10 shows the free body diagram of the inverted pendulum model with constant height. Mg represents the gravity force, f is the reacting force by the ground, and $M\ddot{x}$ is the inertia force created by the acceleration. In addition, this model is not only generating the trajectory for the single support phase but also providing the initial and final condition for the double support phase.

While the robot walks, there is one double support phase between two single support phases, but the linear inverted pendulum is not suitable for the double support phase. Therefore, to keep continuous motion when the phase changing, the polynomial is used to connect the trajectory for the double support phase with initial and final conditions mentioned in the previous paragraph in Fig. 11.

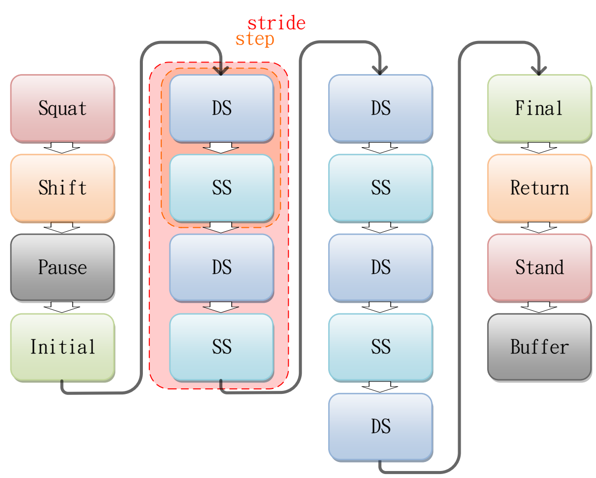

Fig. 12. The flowchart of walking process.

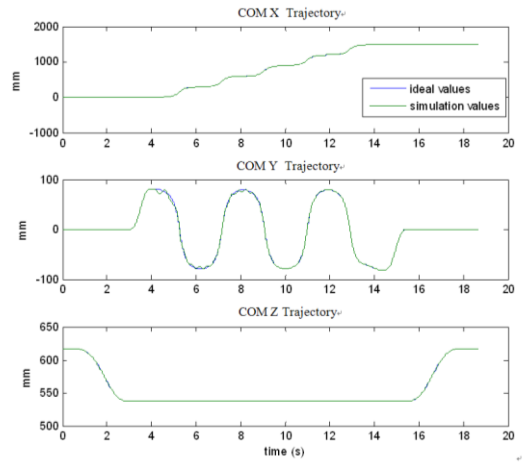

Fig. 13. The plots of the ideal and simulated COM trajectories.

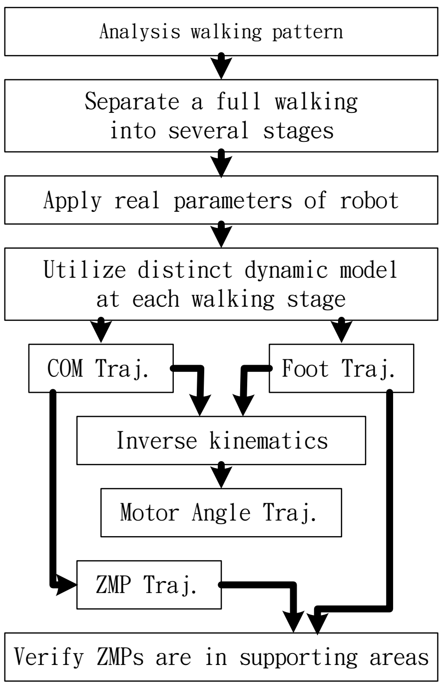

Fig. 14. The flowchart of trajectory planning.

In the whole process of trajectory planning, the first step is to analyze the walking pattern. We separate a full walking into several stages, such as single support (SS) phase, double support (DS) phase, and some steps of adjusting posture at the beginning and at the end of the whole walking period. The steps of adjusting posture include Squat, Shift, Pause, Initial, Final, Return, Stand and Buffer in Fig. 12. Because we use different dynamic model, the time of each step is different, too. The second step is to generate the trajectory of COM (Center Of Mass) in Fig. 13 [16]. The third step is to use the method called Inverse Kinematics to produce the whole trajectory for each motor. However, the third step is not the last one because the final step is to confirm stability of generated trajectory. As the beginning of this section is mentioned, the ZMP of generated trajectory for each motor must be in the support areas, otherwise the designed trajectory will let the robot fall down when robot move on the ground. All of the process of trajectory planning is shown in Fig. 14.

IV. TURNING TRAJECTORY PLANNING

Except for the walking motion, the turning motion is also taken into consideration while robots move on a plane [17-19]. Therefore , here the turning trajectory should be considered for our biped robot. There are three turning modes designed in this paper. The differences between those modes are when the body of robot turns and when the swing leg turns. Initially, the COM and foot trajectories were generated first. Then use Inverse Kinematics to produce the whole turning trajectory for each motor. Last, we confirm stability of generated trajectory.

A. The First Turning Mode: Body Turn First

In the first turning mode, it's divided into 8 steps including Squat, Shift, Body Turn, Leg Turn, Return, Stand Up and Buffer. Figure 15 shows the flowchart. If the robot takes a

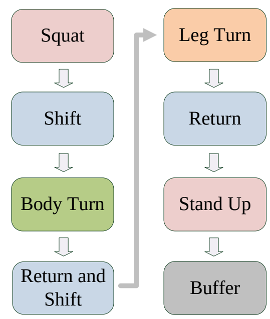

Fig. 15. The flowchart of the first turning mode.

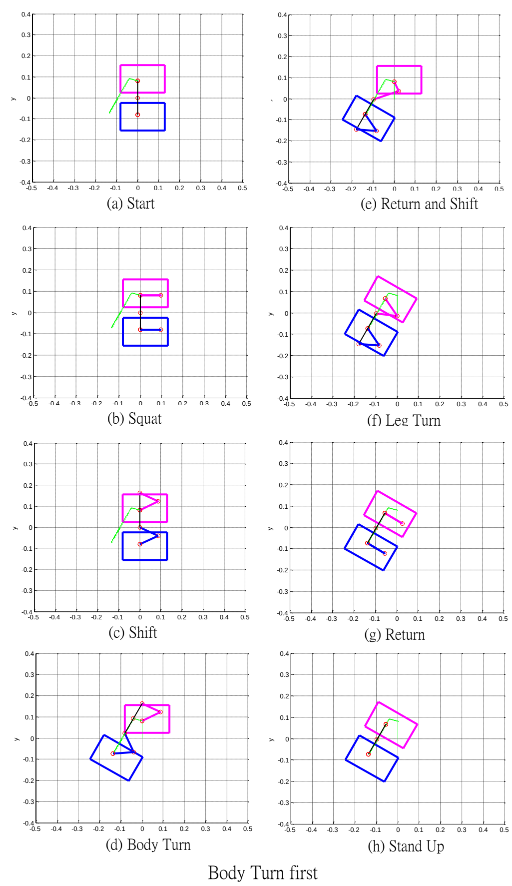

Fig. 16. The top view of the robot taking a 30 degrees right turn in Body Turn First mode.

right turn, the motor of left hip yaw turns to make the body turn right during Body Turn. Then, in Leg Turn, the robot lifts the left leg up and the motor of left hip yaw turns back to make two legs parallel to each other. So, in this turning mode, there is only one motor of hip yaw that turns during the whole turning process. The top view of the robot motion in Body Turn First mode is in Figure 16, and, here the green line means the trajectory of COM.

B. The Second Turning Mode: Leg Turn First

The second turning mode was generated by changing the orders of Body Turn and Leg Turn. The flowchart is in Fig. 17, and the Fig. 18 shows the top view of the robot turning in Leg Turn First mode. In Leg Turn, the motor of right leg hip yaw turns to turn the right leg into new direction. Then the motor of right leg hip yaw turns back and let the body of robot turns in Body Turn. It also only uses one of the two hip yaw motors to

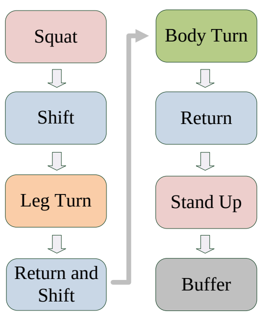

Fig. 17. The flowchart of the second turning mode.

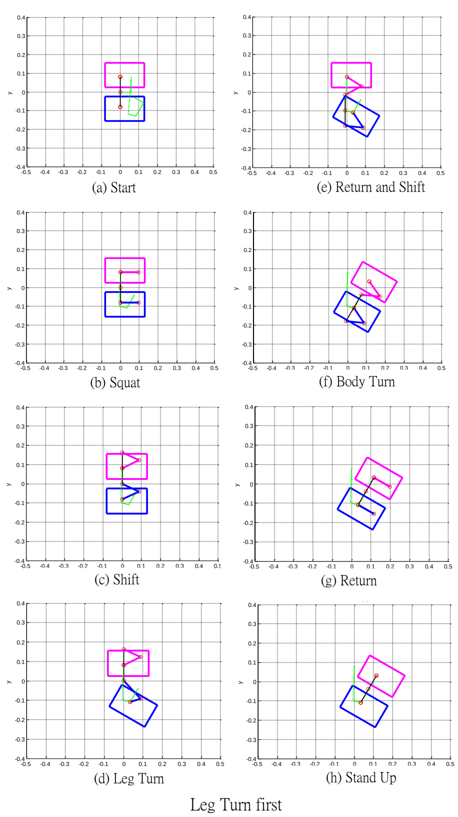

Fig. 18. The top view of the robot taking a 30 degrees right turn in Leg Turn First mode.

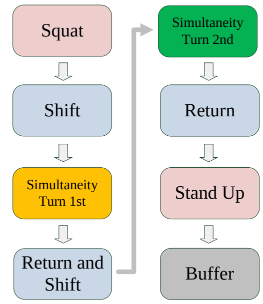

Fig. 19. The flowchart of the third mode.

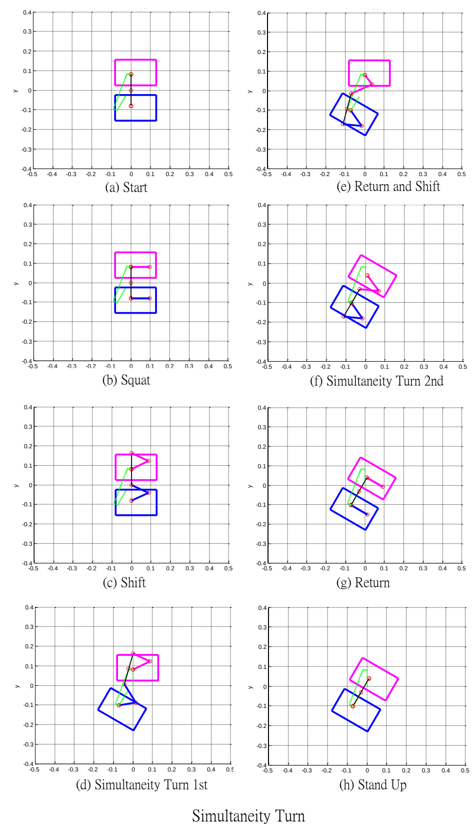

Fig. 20. The top view of the robot taking a 30 degrees right turn in Simultaneity Turn mode.

turn.

C. The Third Turning Mode: Simultaneity Turn

In the design of the biped robot, there are some restrictions in mechanism that limit the work angle of the motor in hip yaw from -40 degrees to 40 degrees. Because of the restriction of mechanism, the maximum angle that robot can turn is under 40 degrees. Therefore, Simultaneity Turn mode is used to make the robot turn more. The flowchart of the third mode is showed in Fig. 19. In Simultaneity Turn mode, if the robot takes a θ turning motion, one of the motors in hip yaw takes a $\theta/2$ turn and the other takes a $-\theta/2$ turn in Simultaneity Turn 1st, and the body takes a $\theta/2$ turn. And in the Simultaneity Turn 2nd, each of those two motors turns back. After Simultaneity Turn 2nd, the robot finishes a whole θ turn. Simultaneity Turn mode could overcome the restriction of mechanism and let the angle that the biped robot is able to turn become twice than the first mode and the second mode. The top view of the robot turning in Simultaneity Turn mode is shown in Fig. 20

V. SIMULATION

When simulating and analyzing motions of a biped robot, the mechanisms model of the robot need to be constructed firstly, and then produce the dynamics model and design controller. To achieve this goal, there are three types of different software applied in the simulation, including SolidWorks, ADAMS, and Matlab. In the full simulation, the first step is to design the mechanism and set the degree of freedoms of biped robot using SolidWorks. In the second step, import the model to ADAMS and set the conditions, such as contact condition, gravity, etc. Finally, export the plant of ADAMS model and use Matlab to control the trajectory for each joint of the biped robot. Figure 21 illustrates the steps of building ADAMS model [20]. Before exporting this dynamic model to Matlab file, there are some variables which are needed to be set. Those variables depend on the input and output of the dynamic plant.

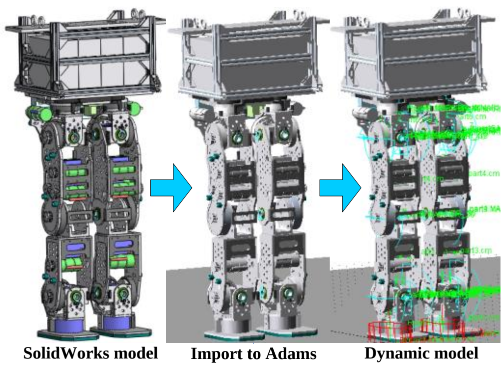

Fig. 21. The steps of building ADAMS model.

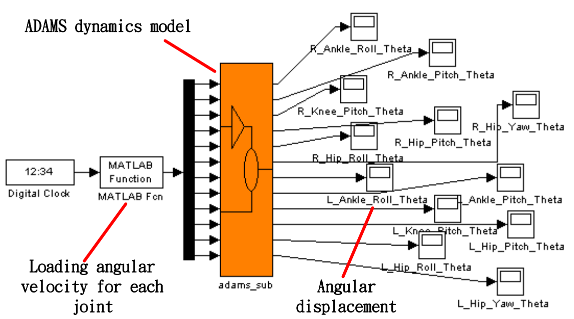

Fig. 22. The Simulink model of controlling ADAMS model with angular velocity input.

There are two types of plant input, angular velocity and torque, used in this paper. Figure 22 shows the Simulink model in Matlab with angular velocity input, and it is assumed the controller and actuator are very powerful without any delay or uncertainty in this simulation, so the trajectories of all joints follow the designed trajectories correctly. The main purpose of this simulation is to test whether the robot can walk stably under the designed trajectory with the contact between soles and ground. Figure 23 demonstrates the snapshots of 3D motion using ADAMS.

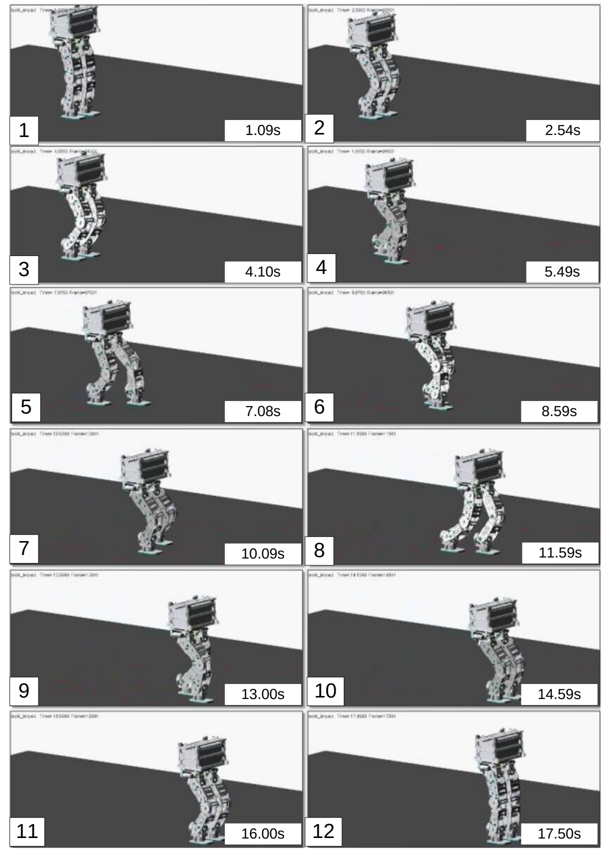

Fig. 23. The snapshots of the robot walking on the flat ground. in ADAMS.

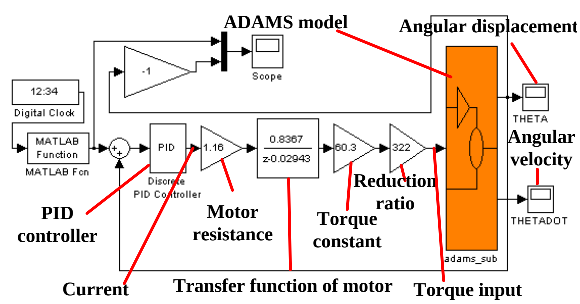

Fig. 24. The Simulink model of controlling ADAMS model with torque input.

On the other hand, Fig. 24 demonstrates the plant which is controlled with torque input for each joint, and it is considered all the parameters of controllers, motors, and reduction ratio to construct the environment of position feedback control. The result of simulation is close to the real situation, but more complicated. Figure 25 shows the walking pattern which the robot's waist is fixed on the supporting mechanism in ADAMS, so the soles will leave the ground while walking. From the result of these situations, it makes sure that the robot can carry out designed walking trajectory stably. Meanwhile, because the design parameters in turning trajectory planning are similar to walking trajectory planning, it can be expected that the robot also can carry out the turning trajectory stably in ADAMS.

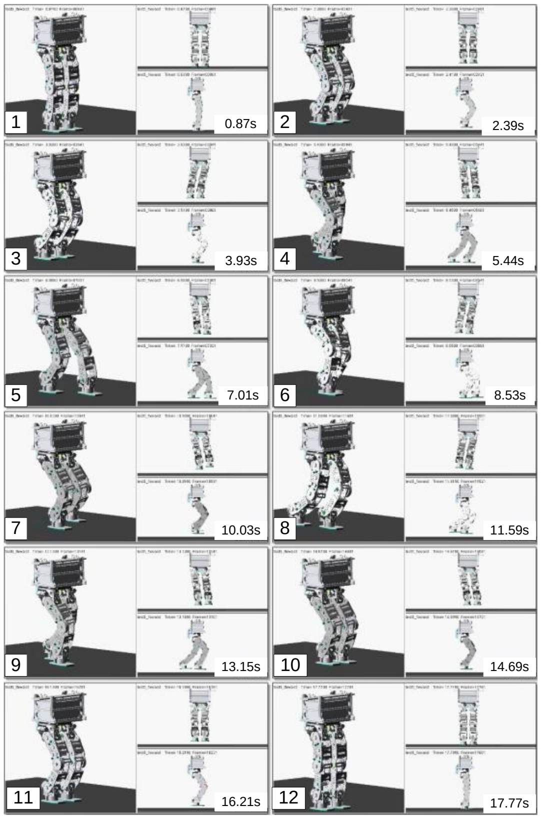

Fig. 25. The snapshots of the robot walking when robot's waist is fixed in ADAMS.

Fig. 26. The snapshots of the robot walking: front view.

VI. Experiment Evaluation

A. Walking Experiments

In the walking Experiments, the effect of clearance from mechanism appears during Single Support step. So, in order to reduce the effect, the motor in hip roll of the support leg needs a compensation of angle. Figure 26 and figure 27 show the snapshots of the walking experiment. Figure 26 is the front view and figure 27 is the side view. After finding the suitable walking parameters, five experiments have been carried out, and those walking parameter are in figure 28. The measurement data of the figure are collected from current sensor and calculated with the parameters. The power efficiency is evaluated according to the "specific resistance" [21], which was determined by weight of the robot, *mg*, its averaged power consumption, *P*, and its averaged forward speed, *v*. It's shown below:

$$S = \frac{P}{mgv}.$$

There are some conclusions in TABLE I, the average power consumption in five experiment is almost the same, and the maximum currents in experiment 2 and 4 are much greater than the other because the clearance compensation need more torque to fix the clearance, in this way, the robot have well landing. The smallest specific resistance of those experiments is experiment 5 because its walk speed is the biggest and the power variation of different experiments is quite small.

Fig. 27. The snapshots of the robot walking: side view.

TABLE I
EXPERIMENT DATA

Comparison					
Experiment Number	1	2	3	4	5
Parameters					
Double Support Period(s)	3.6	3.6	1.8	1.8	3.6
Single Support Period(s)	3.6	3.6	3.6	3.6	3.6
Moving Distance(m/Step)	0.05	0.05	0.05	0.05	0.1
Walking Speed(m/sec)	0.007	0.007	0.009	0.009	0.014
Clearance Compensation	No	Yes	No	Yes	No
Measurement					
Maximum Current(A)	4.48	5.98	4.74	5.70	5.00
Average Current(A)	3.23	3.32	3.29	3.33	3.26
Average Power(W)	155.0	159.1	158.1	159.9	156.6
Specific Resistance	33.49	34.39	25.63	25.91	16.92

Although the specific resistance of experiment 5 is the smallest one, however, it still too big compared with human, and the reasons for the difference between human and robot are well control in every part of human body and energy saving gait of human walking.

B. Turning Experiments

In this section, these three different turning trajectories are carried out by our biped robot. When the robot takes the turning motion, the effect of clearance from mechanism appears, too. Therefore, the motor in hip roll of the support leg still needs a compensation of angle to reduce the effect of clearance. From the data of gyro installed on the robot, the compensation should be about 3 degrees during turning. There

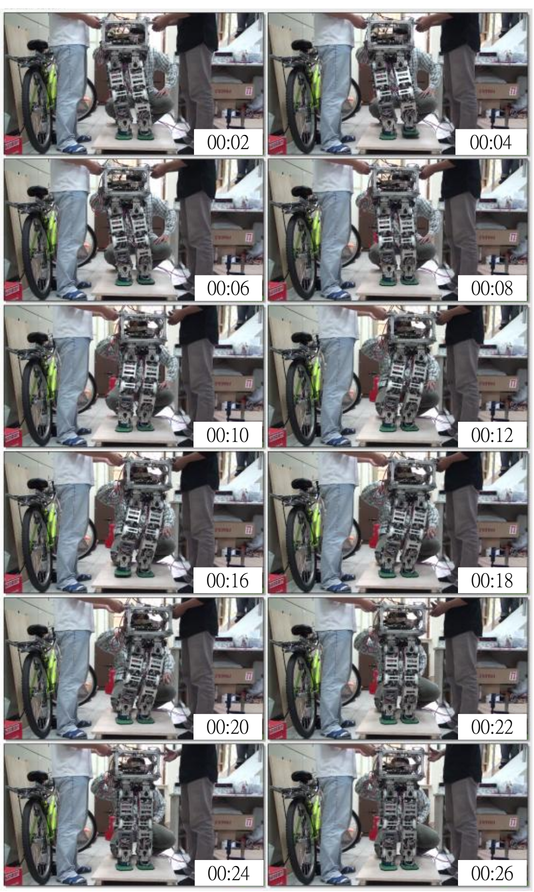

Fig. 28. The snapshots of the robot turning: Body Turn First mode.

Fig. 29. The snapshots of the robot turning: Leg Turn First mode.

Fig. 30. The snapshots of the robot turning: Simultaneity Turn mode.

are three experiments to show the performance of the robot when it takes a 10 degrees left turn. The first turning mode is shown in Fig 28. The results of the second mode and the third mode are shown in Fig.29 and Fig.30.

VII. Conclusion

In this paper we report on the development and system integration of the human-size biped robot. The robot has 12 DOFs, 6 DOFs on each leg. The mechatronic system is customized to fit with commercial embedded system single-board RIO from NI. The walking trajectory is mainly composed of the single support phase with the linear-inverted pendulum model and the stable double-support phase in between. The derived trajectory are simulated in physical engine (Matlab and ADAMS) before the robot experiments, to make sure their stability properties. The robot can successfully walk in the simulation environment. After that, the empirical experiments are executed. The robot can stably walk at 1.08m per minute and can turn 30deg per stride. The performance confirms that development of the human-size biped robot is successful.

We are currently in the process of developing feedback strategy which utilizes the sensory information of 6-axis force transducer and 6-axis IMU; thus the locomotion can be performed in the environment with disturbance.

References

[1] *Honda, Asimo*. Available: http://world.honda.com/ASIMO/

[2] K. Kaneko, F. Kanehiro, S. Kajita, K. Yokoyama, K. Akachi, T. Kawasaki, S. Ota, and T. Isozumi, "Design of prototype humanoid robotics platform for HRP," in *Intelligent Robots and Systems, 2002. IEEE/RSJ International Conference on*, 2002, pp. 2431-2436 vol.3.

[3] K. Kaneko, F. Kanehiro, S. Kajita, H. Hirukawa, T. Kawasaki, M. Hirata, K. Akachi, and T. Isozumi, "Humanoid robot HRP-2," in *Robotics and Automation, 2004. Proceedings. ICRA '04. 2004 IEEE International Conference on*, 2004, pp. 1083-1090 Vol.2.

[4] K. Kaneko, K. Harada, F. Kanehiro, G. Miyamori, and K. Akachi, "Humanoid robot HRP-3," in *Intelligent Robots and Systems, 2008. IROS 2008. IEEE/RSJ International Conference on*, 2008, pp. 2471-2478.

[5] P. Ill-Woo, K. Jung-Yup, P. Seo-Wook, and O. Jun-Ho, "Development of humanoid robot platform KHR-2 (KAIST humanoid robot-2)," in *Humanoid Robots, 2004 4th IEEE/RAS International Conference on*, 2004, pp. 292-310 Vol. 1.

[6] H. J. R. V. T. Inman, and F. Todd., Ed., *Human Walking*. Baltimore,MD: Willams & Wilkins, 1981, p.^pp. Pages.

[7] L. M. Nashner, "Balance adjustments of humans perturbed while walking," *J. Neurophysiol.*, vol. no. 44, pp. 650–664, 1980.

[8] M. Vukobratovic and B. Borovac, "*Zero-moment point — thirty five years of its life*," *International Journal of Humanoid Robotics*, vol. vol. 1, No.1, pp. 147-173, 2004.

[9] C. L. Shih, Y. Z. Li, S. Churng, T. T. Lee, and W. A. Gruver, "Trajectory synthesis and physical admissibility for a biped robot during the single-support phase," in *Robotics and Automation, 1990. Proceedings., 1990 IEEE International Conference on*, 1990, pp. 1646-1652 vol.3.

[10] H. Seung-Suk, Y. Jae-Hyoung, H. Young-Joon, and H. Hern-Soo, "*Natural Gait Generation of Biped Robot based on Analysis of Human's Gait*," in *Smart Manufacturing Application, 2008. ICSMA 2008. International Conference on*, 2008, pp. 30-34.

[11] N. T. Phuong, K. Dae Won, K. Hak Kyeong, and K. Sang Bong, "*An optimal control method for biped robot with stable walking gait*," in *Humanoid Robots, 2008. Humanoids 2008. 8th IEEE-RAS International Conference on*, 2008, pp. 211-218.

[12] H. H. a. Y. F. Zheng, "Dynamics and control of motion on the ground and in the air with application to biped robots," *Journal of Robotic System*, vol. 1, no.1, pp. 101–116, 1984.

[13] R. E. Goddard, Y. F. Zheng, and H. Hemami, "Control of the heel-off to toe-off motion of a dynamic biped gait," *Systems, Man and Cybernetics, IEEE Transactions on*, vol. 22, pp. 92-102, 1992.

[14] T. Buschmann, S. Lohmeier, H. Ulbrich, and F. Pfeiffer, "*Dynamics simulation for a biped robot: modeling and experimental verificatio*n," in *Robotics and Automation, 2006. ICRA 2006. Proceedings 2006 IEEE International Conference on*, 2006, pp. 2673-2678.

[15] H. Hirukawa, F. Kanehiro, S. Kajita, K. Fujiwara, K. Yokoi, K. Kaneko, and K. Harada, "*Experimental evaluation of the dynamic simulation of biped walking of humanoid robots*," in *Robotics and Automation, 2003. Proceedings. ICRA '03. IEEE International Conference on*, 2003, pp. 1640-1645 vol.2.

[16] L. J.-C., "*Gait Generation of a Biped Robot and Construction of measurement system*," Master Thesis, *Department of Mechanical Engineering*, National Taiwan University, 2010.

[17] H. S. Shengjun PENG, Hongxu MA, "A Simulation and Experiment Research on Turning Gait Planning of Blackmann-II Humanoid Robot," presented at the 8th IEEE International Conference on Control and Automation Xiamen, China, 2010.

[18] E. Kim, T. Kim, and J. W. Kim, "Three-dimensional modelling of a humanoid in three planes and a motion scheme of biped turning in standing," *Control Theory & Applications, IET*, vol. 3, pp. 1155-1166, 2009.

[19] S. Kajita, F. Kanehiro, K. Kaneko, K. Fujiwara, K. Yokoi, and H. Hirukawa, "A realtime pattern generator for biped walking," in *Robotics and Automation, 2002. Proceedings. ICRA '02. IEEE International Conference on*, 2002, pp. 31-37 vol.1.

[20] W. S.-F., "*Design and Realization of a Biped Robot*," Master Thesis, *Department of Mechanical Engineering*, National Taiwan University, 2010.

[21] G. Gabrielli, & von Karman, T. H. , "What price speed?," *ASME Mechanical Engineering,*, vol. 72(10), , pp. 775-781., (1950).